

1 Identification of secondary aerosol precursors emitted by an 2 aircraft turbofan

3 Dogushan Kilic^{1,‡}, Imad El Haddad¹, Benjamin T. Brem^{2,5}, Emily Bruns¹, Carlo Bozetti¹, Joel
4 Corbin¹, Lukas Durdina^{2,5}, Ru-Jin Huang¹, Jianhui Jiang¹, Felix Klein¹, Avi Lavi⁴, Simone M.
5 Pieber¹, Theo Rindlisbacher³, Yinon Rudich⁴, Jay G. Slowik¹, Jing Wang^{2,5}, Urs
6 Baltensperger¹, and Andre S. H. Prévôt¹

7 ¹Laboratory of Atmospheric Chemistry, Paul Scherrer Institute, Villigen PSI, 5400, Switzerland

8 ²Laboratory for Advanced Analytical Technologies, Empa, Dübendorf, 8600, Switzerland

9 ³Federal Office of Civil Aviation, Bern, 3003, Switzerland

10 ⁴Department of Earth and Planetary Sciences, Weizmann Institute of Science - Rehovot – Israel

11 ⁵Institute of Environmental Engineering, ETH Zurich, Zurich, 8093, Switzerland

12 [‡] Now at: Istanbul Technical University, Eurasian Institute of Earth Sciences, Maslak, 34469, Turkey

13 *Correspondence to:* andre.prevot@psi.ch and imad.el-haddad@psi.ch

14 **Abstract.** Oxidative processing of aircraft turbine-engine exhaust was studied using a potential aerosol mass
15 (PAM) chamber at different engine loads corresponding to typical flight operations. Measurements were
16 conducted at an engine test cell. Organic gases (OGs) and particle emissions pre/post PAM were measured. A
17 suite of instruments, including a proton-transfer-reaction mass spectrometer (PTR-MS) for OGs, a multi-gas
18 analyzer for CO, CO₂, NO_x, and an aerosol mass spectrometer (AMS) for non-refractory particulate matter (NR-
19 PM₁) were used. Total aerosol mass was dominated by secondary aerosol formation, which was approximately
20 two orders of magnitude higher than the primary aerosol. The chemical composition of both gaseous and particle
21 emissions were also monitored at different engine loads and were thrust-dependent. At idling load (thrust 2.5-
22 7%), more than 90% of the secondary particle mass was organic and could be explained by the oxidation of
23 gaseous aromatic species/ OGs; *e.g.* benzene, toluene, xylenes, tri-, tetra-, and pentamethyl-benzene and
24 naphthalene. The oxygenated-aromatics, *e.g.* phenol, furans, were also included in this aromatic fraction and their
25 oxidation could alone explain up to 25% of the secondary organic particle mass at idling loads. The organic
26 fraction decreased with thrust level, while the inorganic fraction increased. At an approximated cruise load sulfates
27 comprised 85% of the total secondary particle mass.

28 1 Introduction

29 Airport activities emit both particulate and gaseous emissions (Unal et al., 2005; Hudda et al., 2014), and are a
30 significant source of local gas- and particle-phase pollutants (Westerdahl et al., 2008). These emissions affect
31 public health (Lin et al., 2008) and local air quality by increasing pollutant concentrations, *e.g.* ultrafine particulate
32 matter (PM) number concentrations, at the surrounding residential areas (Hudda and Fruin, 2016; Hudda et al.,
33 2016).

34 The dominant source of airport aerosol is aircraft engine exhaust (Kim, 2009), and is classified as either directly
35 emitted primary aerosol (PA) or secondary aerosol (SA). Due to the high combustion efficiency, PA from aircraft
36 engines contains mainly black carbon (BC) whereas SA is formed by the oxidation of emitted precursor gases.
37 PA and SA precursor emissions such as non-methane organic gases (NMOGs) strongly depend on aircraft engine
38 operating conditions (Kinsey et al., 2010) *e.g.* the BC emission index (EI, g/kg fuel) of a gas-turbine engine is
39 usually higher at cruise climb-out and take-off loads (above 60% of the maximum thrust) than at lower loads used
40 at idle, taxi (7%) and approach (30%) (Liati et al., 2014; Brem et al., 2015). In contrast to BC, NMOG emissions,
41 including *e.g.* aromatic hydrocarbons, aliphatic hydrocarbons and carbonyls, are clearly highest at low loads
42 (Spicer et al., 1994; Slemr et al., 2001; Anderson et al., 2006; Herndon et al., 2006; Kilic et al., 2017).

43 Aging of fossil fuel combustion exhaust leads to SA/PA ratios higher than 1. Single-ring aromatics are
44 traditionally thought to be the most important secondary organic aerosol (SOA) precursors from combustion
45 emissions. While this has been shown to be the case for some emissions, *e.g.* from 2-stroke engines (Platt et al.,
46 2014), in other cases non-traditional precursors were assessed to be responsible for the bulk of the SOA mass
47 formed, *e.g.* for biomass smoke (Bruns et al., 2016) or on-road vehicles (Platt et al., 2013; 2017; Pieber et al.,
48 2017). Similar to these emissions, aging of aircraft emissions studied by Miracolo et al. (2011; 2012) in a smog
49 chamber produced substantial amounts of secondary PM exceeding primary PM emissions several-fold. The
50 authors showed the dominance of secondary organic aerosol (SOA) at low loads, while at high loads sulfate was
51 the main SA produced. While single-ring aromatic compounds determined using gas-chromatography/mass

52 spectrometry seemed to be important precursors of the SOA formed, a greater part of SOA was believed to
53 originate from non-traditional precursors, whose nature remains to be identified (Miracolo et al., 2011; 2012).
54 In this study, we measured the SA production potential of aircraft jet engine exhaust as a function of engine load
55 and examined the bulk gas-phase organic emissions and their SOA formation potential. SOA was produced by
56 OH-initiated oxidation of aircraft NMOG emissions in a potential aerosol mass (PAM) flow reactor (Kang et al.,
57 2007). Primary and secondary PM mass was characterized for different engine loads, using an aerosol mass
58 spectrometer (AMS). SOA precursors were analyzed in real-time by a proton-transfer-reaction mass spectrometer
59 (PTR-MS) and SOA closure was examined under different conditions. The impact of these emissions and their
60 SOA potential in typical urban atmospheres, at the proximity of airports is assessed and compared to other mobile
61 sources.

62 **2 Methods**

63 **2.1 Experimental setup**

64 Exhaust measurements were conducted to characterize NMOG and non-refractory submicron particulate mass
65 (NR-PM₁) emissions from an in-production CFM56 variant turbofan in the test cell of SR Technics at Zurich
66 Airport. The test engine was fueled with standard JET A-1 fuel (see Table S1 for specifications), and was operated
67 at several engine loads, selected to represent aircraft activities during a typical landing/take-off (LTO) cycle.
68 Engine loads were set by specifying the combustion chamber inlet temperature values which correlate with a
69 specific thrust (lbf) at standard atmospheric conditions. The selected loads included idle-taxi (3-7% of the
70 maximum thrust), approach (30% of the maximum thrust), and an approximated cruise load (50-65% of the
71 maximum static thrust). After starting the engine, a warm-up sequence of 25 minutes ran before each test,
72 consisting of five minute-long steps at thrusts of 5%, 15%, 7%, 65% and 85% in sequence.

73 A simplified scheme of the experimental setup is shown in Figure 1 and is discussed in detail elsewhere (Kilic et
74 al., 2017). Details about the sampling system for non-volatile particle emissions can be found in Durdina et al.
75 (2017) and Brem et al. (2015). The turbine engine exhaust was sampled by a single-point probe with an inner
76 diameter of 8 mm, located 0.7 m downstream of the engine exit plane. At this sampling location, the lubricant oil
77 contribution to the exhaust is expected to be minimal (only due to leaking hydrodynamic seals at startup/idle)
78 compared to the runway measurements since the engine design studied does not vent lubricant oil through its core
79 (where probe pulled sample). The exhaust drawn by the probe was directed through a heated (160°C) transfer line
80 to three different lines: (i) the raw gas line, (ii) diluted emissions line and (iii) diluted aged emissions line. CO,
81 CO₂, and NO_x were measured by a multi-gas analyzer (PG250, Horiba Inc.) installed on the raw line. On the
82 diluted line, primary gas and particle measurements were performed. Two ejector dilutors (DEKATI DI-1000)
83 were installed in sequence on this transfer line; after the first dilution, sampling lines were heated to 120°C. The
84 sample was diluted with synthetic air (99.999% purity) either by a factor of 10 or 100, depending on the NMOG
85 concentration. The NMOGs were quantified and characterized by a proton-transfer-reaction time-of-flight mass
86 spectrometer (PTR-ToF-MS) together with a flame ionization hydrocarbon detector (FID) (APHA 370 THC
87 Monitor). The concentration of equivalent black carbon (BC) was determined by a 7-wavelength aethalometer
88 (Drinovec et al., 2015) based on optical absorption.

89 Aging of the engine exhaust emissions was achieved by using a potential aerosol mass (PAM) chamber with a
90 continuous flow of 7.6 l/min and a volume of 13.3 liters. Two mercury lamps (emission lines at wavelengths
91 $\lambda=182$ nm – 254 nm, BHK Inc.), mounted inside the PAM, were used to irradiate HONO and O₂ required for
92 hydroxyl radical (OH) formation. Different time-integrated OH exposures (molecules cm⁻³ h) were achieved by
93 modulating UV lamp intensity *e.g.* 80%, 90%, 100%. HONO to boost OH concentrations, and D9-butanol to trace
94 OH exposure (Barnet et al., 2012), were injected with flows of 1.8 and 0.4 l/min, respectively. Further, the PAM
95 was also humidified (~20% relative humidity) by injecting synthetic air with water vapor (with a flow of 1.6
96 l/min). All measurements were conducted at 295-298°K. Secondary aerosol formation was measured after the
97 PAM, while the primary emissions were measured from the bypass line.

98 Aging in a PAM is not completely analogous to that in a smog chamber, due to higher oxidant concentrations.
99 However, intercomparison studies suggest that the amount of SOA production and its bulk elemental composition
100 are comparable for both single precursors (*e.g.* α -pinene) (Lambe et al., 2015) and complex emissions (*e.g.* wood
101 combustion) (Bruns et al, 2015). In addition, in both the PAM and chambers, the dominant oxidation pathways
102 are similar to those in ambient air (Peng et al, 2015; 2016).

103 **2.2 Instrumentation**

104 **2.2.1 PTR-ToF-MS**

105 NMOGs having a higher proton affinity than water were quantified by a PTR-ToF-MS (PTR-TOF 8000, Ionicon
106 Analytik G.m.b.H., Innsbruck, Austria) (Jordan et al., 2009). NMOG molecules were positively charged in the
107 ionization unit (drift tube) of the instrument via hydronium ions (H₃O⁺), and the generated ions/fragments were
108 measured by a time-of-flight mass spectrometer. The PTR-ToF-MS utilized a drift voltage (Udrift) of 550 V, a

109 drift chamber temperature (T_{drift}) of 60°C and a drift pressure (p_{drift}) of 2.2 mbar, maintaining a reduced electric
110 field (E/N) of ~120 Townsends (Td). Data were collected with one second time resolution.
111 Tofware post-processing software (version 2.4.5, TOFWERK AG, Thun, Switzerland; PTR module as distributed
112 by Ionicon Analytik GmbH, Innsbruck, Austria), running in the Igor Pro 6.3 environment (Wavemetrics Inc., Lake
113 Oswego, OR, USA), was used for data analysis. The ion transmission function, required to convert counts (cps)
114 to volume mixing ratios (ppbv), was quantified using a gas standard containing a mixture of 12 compounds (100
115 ppbv each) spanning mass-to-charge ratios (m/z) from m/z 33 to 181 (Carbagas AG., Zurich, Switzerland). Volume
116 mixing ratios (ppbv) were calculated according to De Gouw and Warneke, 2007, using $\text{H}_3\text{O}^+/\text{NMOG}$ reaction rate
117 constants (k) from Cappellin et al., 2012, when available, and assuming $2 \times 10^{-9} \text{ cm}^3 \text{ s}^{-1}$ otherwise.
118 During the exothermic proton-transfer reaction, some molecular fragments are formed in the drift chamber, with
119 the extent of fragmentation depending on the chamber conditions and functional groups in the molecules
120 (Gueron et al., 2015). In particular, hydrocarbon fragments are obtained from aldehydes and dehydration of
121 some oxygenated ions. Assignment of these fragment ions to the corresponding parent ions is important for
122 quantification. The NMOG mixing ratios were corrected by accounting for this fragmentation. The compounds
123 were measured based on their parent ions, then their fragments were subtracted based on reference fragmentation
124 patterns. These subtractions combine a detailed fragmentation table for aldehydes using the current drift chamber
125 conditions from Klein et al. (2016) and fragmentation patterns for aromatic compounds measured under similar
126 chamber conditions reported ($E/N \sim 120$ Td) in other studies (Buhr et al., 2002; Brown et al., 2010; Gueron et
127 al., 2015). The fragmentation of detected compounds containing other functional groups (*e.g.* hydrocarbons and
128 non-aldehyde oxygenated compounds) cannot be fully excluded but are not expected to cause significant error
129 since the observed parent molecules were primarily low molecular weight alcohols and acids (*e.g.* methanol,
130 formic and acetic acid) that are less susceptible to fragmentation (de Gouw and Warneke, 2007). The NMOGs
131 were then classified (acids, alcohols, aromatics, non-aromatics hydrocarbons and unclassified hydrocarbon
132 fragments, nitrogen and sulfur containing compounds, other oxygen containing compounds, unidentified peaks)
133 according to Kilic et al. (2017).

134 2.2.2 AMS

135 The condensed phase was continuously monitored before and after the PAM using a high resolution time-of-flight
136 aerosol mass spectrometer (AMS) and a scanning mobility particle sizer (SMPS). The reader is referred to DeCarlo
137 et al. (2006) for a more detailed description of the AMS operating principles, calibrations protocols, and analysis
138 procedures. Briefly, a particle beam sampled through an aerodynamic lens is alternately blocked and unblocked,
139 yielding the bulk particle mass spectra (MS mode) of the non-refractory (NR) species, including organic aerosols
140 (OA), NO_3^- , SO_4^{2-} , NH_4^+ , and Cl^- . The NR particles are flash vaporized by impaction on a heated tungsten surface
141 (heated to ~ 600°C) at ~ 10^{-7} Torr. The resulting gases are ionized by electron ionization (EI, 70 eV) and the
142 mass-to-charge ratios (m/z) of the fragments are determined by the ToF mass spectrometer. The AMS was
143 operated in the V-mode, with a time resolution of 30 sec. The AMS data were analyzed using the SQUIRREL
144 (version 1.52L) and PIKA (1.11L) analysis software in Igor Pro 6.3 (WaveMetrics). Standard relative ionization
145 efficiencies (RIE) were assumed for the organic aerosol and chloride (RIE = 1.4, and 1.3, respectively) and
146 experimentally determined for sulfate and ammonium (RIE = ~1.1 and ~4, respectively). The collection
147 efficiency due to the particle bounce was determined to be ~1 under our conditions for organic rich aerosols by
148 comparing the AMS mass to the SMPS volume (assuming an OA density of 1.4).

149 For aged emissions, the CE was estimated by comparing the particle mass calculated by the AMS + BC with that
150 estimated using the SMPS. For both thrust settings, the CE is not significantly different than 1. This is because at
151 low thrust the aged particles consist mostly of organic matter, which had been shown to be efficiently collected
152 on the vaporizer for chamber aerosols (Stirnweis et al., 2017, Platt et al., 2017). Meanwhile, the aged aerosol at
153 higher thrust settings is predominantly composed of sulfuric acid; the molar ratio between NH_3 and SO_4 is ~0.3,
154 while fully neutralized ammonium sulfate would have a ratio of 2. As opposed to ammonium sulfate, sulfuric acid
155 is efficiently collect on the vaporizer. Therefore, we concluded that using CE=1 for all thrust levels is adequate.
156 We note that because of the high contribution of the BC to fresh emissions, we could not determine the CE of
157 primary OA and we used CE=1. Such CE is expected for hydrocarbon like particles.

158 2.3 Data analysis

159 Emissions from the aircraft turbofan were measured at different thrust levels referred to as “test points”
160 hereinafter. Test point durations were 18 minutes, except for one 60 minute-long run. Test points were
161 systematically interspersed with five minute-long periods to clean the PAM and the transfer lines by flushing the
162 setup with synthetic air. The averaging of the primary emissions started from the third minute of a test point when
163 the engine operation was stable. After sampling primary emissions for five to eight minutes while bypassing the
164 PAM, secondary formation was measured after the PAM during the last five to eight minutes of the test point.
165 This allows SOA to reach a steady state in the PAM. During each test, the PA concentration was measured by

166 bypassing the PAM, while the SA concentration was calculated by subtracting PA from the OA measured after
 167 aging (after the PAM). Both PA and SA concentrations were determined by AMS.
 168 The expected SOA concentration from the sum of all NMOGs detected by the PTR-ToF-MS was also calculated
 169 by multiplying the NMOGs oxidized in the PAM by its corresponding SOA yields, according to Eq. 1:

$$170 \quad \sum_{i=1}^n SOA \text{ modelled} = \sum_{i=1}^n \Delta NMOG_i \times Yield_i \quad \text{Eq. 1,}$$

171 where n is the number of NMOGs quantified and $\Delta NMOG$ is the difference between the primary NMOG
 172 concentration and the NMOG concentration after aging. The same approach was applied by Bruns et al. (2016)
 173 and yields used can be found in Table 2. SOA yields available in the literature were used when possible.
 174 Otherwise, SOA yields of 0.2 were assumed as a lower limit estimate for aromatic and oxy-aromatics for which
 175 no SOA-yield values were reported (Presto et al., 2010; Tkacik et al., 2012), similar to Bruns et al. (2016). A yield
 176 of 0.15 was assumed for other NMOGs, including non-aromatic hydrocarbons and carbonyls. As NO is completely
 177 consumed in the PAM, we have chosen yields from low NO_x conditions for aromatic hydrocarbons (Ng et al.,
 178 2007; Chan et al., 2009; Hildebrandt et al., 2009; Nakao et al., 2011). The SOA contribution from organic gases
 179 lighter than benzene (C₆H₆) was neglected. Predicted NMOG contributions to SOA are provided in the Results
 180 section.

181 Emission indices (EI , g/kg fuel) were calculated using a mass balance on fuel carbon:

$$182 \quad EI = [X] \times \left[\frac{MW_{CO_2}}{MW_C \times \Delta CO_2} + \frac{MW_{CO}}{MW_C \times \Delta CO} \right] \times C_f \quad \text{Eq. 1,}$$

183 where X denotes the pollutant concentration ($\mu\text{g}/\text{m}^3$) and MW (g/mole) is the molecular weight of the species
 184 denoted by the subscript. Background-subtracted CO and CO₂ concentrations ($\mu\text{g}/\text{m}^3$) are denoted as ΔCO and
 185 ΔCO_2 , respectively. C_f is the carbon fraction of the JET-A1 fuel used during the campaign and was measured as
 186 0.857 based on ASTM D 5291 method (ASTM, 1996).

187 Particle losses to the PAM wall were taken into account during particle mass calculations by measuring primary
 188 emissions of NR-PM₁, with lights off, before and after the PAM. From this test, we estimated the losses to the
 189 PAM walls to be ~5%, consistent with previous studies (Bruns et al. 2015, Palm et al. 2016). All data presented
 190 were corrected for particle wall losses.

191

192 **3 Results and discussion**

193 **3.1 SOA formation as a function of OH exposure**

194 The evolution of the chemical composition of the primary organic gases and NR-PM₁ components with increasing
 195 OH exposure is shown in Figure 2 for engine idling operation (thrust 3%). Measurements were conducted for
 196 primary emissions, as well as for OH exposures of 59×10^6 , 88×10^6 , and 113×10^6 molecules $\text{cm}^{-3} \text{ h}$, which
 197 correspond to approximately 39, 58, and 75 hours of atmospheric aging under an average tropospheric OH
 198 concentration of 1.5×10^6 molecules cm^{-3} (Mao et al., 2009). The OH exposure, calculated using d9-butanol as a
 199 tracer, was varied by varying the light intensity.

200 Figure 2 shows the OG composition under these conditions with compounds classified as a function of their
 201 molecular composition, as described in Kilic et al. (2017). A stepwise increase of the OH exposure reduced the
 202 NMOG mass detected in the chamber by 35%, 40% and 50%. Except for carboxylic acids, the concentrations of
 203 all NMOGs decreased during aging, indicating that their loss rate exceed their production from other NMOGs.
 204 For example, aromatic compounds and carbonyls were oxidized in the PAM by up to 90% and 50%, respectively,
 205 while the acids doubled after 75 hours of daytime-equivalent aging.

206 Figure 2 also shows a time series of secondary NR-PM₁ composition, as well as the concentrations of two of the
 207 most abundant aromatic gases, C₁₀H₁₄ and C₁₁H₁₆, for the same experiment. Here stable oxidation conditions were
 208 alternated with sampling of primary emissions, with OH exposures indicated in the figure. Secondary aerosol,
 209 especially SOA, dominated the total NR-PM₁. By increasing the OH exposure from 59×10^6 to 88×10^6 , the
 210 generated SOA increased by approximately 14%. However, increasing the OH exposure further to 113×10^6
 211 molecules $\text{cm}^{-3} \text{ h}$ yielded only an additional 3% increase in SOA mass. This suggests that at these OH exposures,
 212 the bulk of SOA precursors have reacted and the additional SOA production did not significantly exceed its loss.
 213 Under these conditions, the formed SOA may be considered as a reasonable estimate for the total SOA potential.
 214 The observed production rate of SOA against OH exposure is consistent with precursor reaction rates of 8×10^{-12}

215 molecule⁻¹ cm³ s⁻¹. This estimate is based on the assumption of a constant SOA mass yield with aging and
216 instantaneous equilibrium partitioning of the condensable gases, and is therefore lower than the reaction rates of
217 the main identified precursors (see below). SOA production rates are thus expected to be faster in the ambient
218 atmosphere.

219 3.2 Particle and gaseous emissions as a function of engine load

220 Figure 3 shows both average primary and secondary emissions indices for varying engine loads (left) and EIs
221 from individual test points (right). The NMOG EI decreased from 30 to 0.8 g/kg fuel when the thrust level
222 increased from 3-5% to 90%. At thrust 3-5%, the emissions of gaseous aromatic-hydrocarbons were highest (with
223 an EI of ~5g/kg fuel) and decreased with increasing thrust (with an EI of ~0.15 g/kg fuel at thrust 90%). Similar
224 to aromatic gases, SOA were formed mostly at 3-5% thrust and had a declining trend with thrust. In contrast, BC,
225 POA and secondary SO₄ EIs were highest during the approximated cruise load (thrust 60%). At these conditions,
226 secondary NR-PM₁ was mostly inorganic and SOA mass was comparable to that of primary carbonaceous
227 emissions (BC + POA). SOA was approximately 100 times higher than POA at idle and only 10 times higher at
228 cruise (Figure 3). This dependence of the aged aerosol composition on the thrust level, obtained using the PAM
229 reactor, confirm quite readily the previous results obtained in a smog chamber (Miracolo et al., 2011; 2012).

230 There is a PM fraction in the engine exhaust originating from the lubricant oil (Yu et al., 2012) that is not measured
231 due to the sampling location and engine model studied. The EI of this PM fraction ranges in 2 – 10 mg/kg fuel
232 (Yu et al, 2010) for other engine models than the engine model studied here. This PM originating from lubricant
233 oil is less than 1% of the SOA at idle however it could be a significant source at cruise loads.

234 3.3 Precursor gases of SOA: Idling

235 Single-ring aromatics, such as xylenes, methylbenzenes, toluene, and benzene, were previously linked with SOA
236 formation (*e.g.*(Odum et al., 1997; Ng et al, 2007)). These aromatic gases are important contributors in the
237 emissions from combustion sources such as two-stroke scooters (Platt et al., 2013), or wood burning (Bruns et al.,
238 2016). Idling exhaust contained 20% (mass weighted) of aromatic HCs. Figure 4 presents the mass fractions of
239 aromatic hydrocarbons in primary exhaust for an idling turbine engine. More than half of the aromatic
240 hydrocarbons emitted were single-ring aromatics. 75 - 95% of these aromatics were oxidized with an OH exposure
241 of ~90 x 10⁶ molecules cm⁻³ h in the PAM.

242 By using previously reported SOA yields (Table 2) for NMOGs, SOA production was predicted from individual
243 precursors according to Eq. 1. Figure 5 shows a comparison of the predicted SOA with the SOA determined by
244 AMS measurements (top) and the predicted SOA contribution by the oxidation of NMOGs in the PAM (bottom),
245 for two idling thrusts, 2-5% (left) and 6-7% (right). The predicted SOA from the NMOGs reacted are shown at
246 the bottom panel of the figure and compound class-specific SOA fractions are separated for aromatic HCs,
247 oxygenated-aromatics, other HCs, N-containing OGs and other OGs.

248 SOA yields are sensitive to the conditions at which the experiments were conducted. Parameters that can have an
249 influence on SOA yield determination include among others the NO_x/VOC ratio and the particle condensational
250 sink and mass concentrations. Under our conditions, the PAM is operated under low NO_x/VOC conditions and at
251 rather high condensational sinks; both conditions would favor higher yields (Stirnweis et al. 2017). We have
252 attempted to use yields from studies conducted under similar conditions. However, we note that reported yields
253 for similar conditions may vary by up to a factor of two.

254 Results in Figure 5 indicate that the most important SOA precursors emitted by turbine engines at idle are aromatic
255 hydrocarbons such as benzene derivatives but also oxygenated aromatics such as phenol. The predicted SOA
256 formed by aromatics alone, both by aromatic hydrocarbons (60-70%) and oxygenated-aromatics (15-25%),
257 explained all AMS-determined SOA at low loads (thrust 3-5%) and most of the SOA formed (by 80%) at idle 6-
258 7% (Figure 5). Predicted aromatic SOA from benzene (C₆H₆), C2-benzenes (C₈H₁₀), C3-benzenes (C₉H₁₂), C4-
259 benzenes (C₁₀H₁₄), dimethylstyrenes (C₁₀H₁₂), toluene (C₇H₈), methylbenzaldehydes (C₈H₈O) and phenol
260 (C₆H₆O) accounted for 60% of the AMS-determined SOA at 3-5% thrust (Figure 5). These results are consistent
261 with those previously obtained using a smog chamber, confirming that aromatic compounds are indeed important
262 SOA precursors in jet-engine emissions (Miracolo et al., 2011). Only a small fraction of these compounds was
263 determined in previous experiments using GC/MS measurements and therefore traditionally considered as SOA
264 precursors in models. Here, compared to previous experiments we show that non-traditional aromatic and oxy-
265 aromatic compounds, including naphthalene and its alkyl derivatives, C>3 alkyl derivatives of single ring
266 aromatics, and phenols, can explain the gap between measured SOA and SOA predicted based on traditional
267 precursors.

268 Exhaust-aging experiments were repeated 6 times at thrust 3-5% and the oxidation of NMOGs varied during each
269 of these aging experiments. Error bars shown in Figure 5 denote this variability in NMOG oxidation (in the PAM)
270 during aging experiments of the same thrust level. Indeed, errors related to yield values used may significantly
271 influence the results. These errors may be systematic and are complex to assess. They can be affected by potential
272 differences between the oxidation conditions in chambers and in the PAM (*e.g.* NO_x, RH, particle mass). Yields

273 obtained with the PAM are consistent with those obtained from chambers (Bruns et al., 2015), therefore we do
274 not expect large systematic errors in the SOA predicted. However, based on the variability of yields in previous
275 chamber experiments we estimate the accuracy of our prediction to be within a factor of 2, indicating that within
276 our uncertainties a significant fraction of the precursors was identified.
277 NMOGs, including aromatic gases, were reduced with increasing thrust (from thrust 3-5% to thrust 6-7%) due to
278 more efficient operation of the turbine engine. This decrease amounted to 40% for the sum of aromatic HCs and
279 corresponded to a 30% decrease in SOA EI. Therefore, a more efficient engine operation implies less NMOG
280 emissions and reduced SOA formation potential at idle.

281 **3.4 SOA formation at an approximated cruise load**

282 A comparison of the predicted SOA with the SOA determined by the AMS is presented in Figure 6 at cruise loads
283 (top panel). Figure 6 also shows the SOA contribution predicted by the oxidation of NMOGs in the PAM (bottom
284 panel) under the same engine conditions. The SOA EI was 0.07 g/kg fuel for cruise load. The predicted SOA
285 fraction accounted for only 30% of the AMS-determined SOA (green bar, Figure 6) during cruise load
286 experiments. Aromatic SOA (predicted) accounted for only 4% of the AMS-determined SOA during these
287 experiments. The major fraction of the remaining SOA mass that was assigned to the identified precursors was
288 predicted to be from oxygenated NMOG molecules (Figure 6). Another 6% of the determined SOA may originate
289 from non-aromatic HCs (aliphatics and HC fragments > C6).

290 Predicted SOA was significantly lower compared to the measured SOA. While SOA precursors remain
291 unidentified under these conditions, several hypotheses might explain the observation. First, we could not
292 determine the contribution of alkanes smaller than 9 carbon atoms to the formed SOA, because these compounds
293 are not directly detected by the PTR-ToF-MS. Depending on the number of carbon atoms in their molecular
294 structure, the SOA potential of many alkanes may be comparable to that of single-ring aromatic hydrocarbons
295 (Tkacik et al., 2012) and therefore may play a role in the formation of the observed SOA. However, our data do
296 not suggest that a great part of the observed SOA is from non-measured alkanes, as we do not observe any increase
297 in the contribution of hydrocarbon fragments in the PTR-MS compared to idling emissions. Second, the oxidation
298 of primary semi-volatile compounds may yield significant SOA, because of their elevated yields of near unity
299 (Robinson et al., 2007). However, we note that these semi-volatile precursors would play an important role at low
300 aerosol concentrations, when most of these precursors reside in the gas-phase where they can be oxidized. Under
301 our conditions, concentrations range between 10 and 50 $\mu\text{g m}^{-3}$ and a substantial fraction of these products resides
302 already in the particle phase. Therefore the oxidation of these products in the gas-phase by OH is unlikely to
303 explain the observed entire 10-fold increase in the OA mass upon oxidation, but only part of the mass. Finally,
304 the PTR-MS data suggest that a great part of the precursors measured are highly oxygenated gases, with O:C
305 ratios ranging from 0.2 to 0.7, including, among others, anhydrides (*e.g.* phthalic, succinic and maleic) and
306 quinone derivatives. Unlike aromatic compounds and alkanes present in the fuel, these compounds are likely
307 formed at high temperature during combustion. The SOA yields of these compounds remain unknown and it is
308 likely that the yield value of 0.15 used here is a lower estimate, which would result in an underestimation of the
309 contribution of these compounds to the observed SOA. We also note that unlike precursors detected under idle
310 conditions, the ionization efficiency and the fragmentation pattern of these compounds in the PTR-MS are highly
311 uncertain, resulting in large uncertainties in our predicted SOA. Therefore, results in Figure 6 should be considered
312 with care. Notwithstanding these uncertainties, we note that at cruise conditions the SOA contribution to the total
313 secondary PM is minor compared to sulfate and therefore these uncertainties have little impact on the implications
314 of our results.

315 **4 Conclusions and implications for ambient air quality**

316 Gas-phase, primary emissions and SA formation from an in-service turbofan were investigated in a test cell. The
317 engine loads (thrusts) during the experiments simulated different aircraft operations. These operations are
318 summarized as landing take-off (LTO) cycle under four modes: taxi/idle, approach, climb and take-off with
319 corresponding engine loads of 3-7%, 30%, 85% and 100%, respectively. In addition, an approximated cruising
320 load (60%) was selected.

321 At idle conditions, SOA formation was mostly attributed to the oxidative processing of aromatic precursors.
322 Benzene derivatives together with phenol are the major SOA precursors for an idling aircraft. During cruise load,
323 the emission of aromatic compounds was much lower and only explained a minor fraction of SOA (4%). During
324 these conditions, however, sulfate dominated SA, contributing ~85% of the total mass of aged aerosols and
325 therefore its fraction is more relevant aloft.

326 The oxidation of NMOGs in the PAM yielded a SOA EI 100 times greater than POA under idling conditions and
327 10 times greater at cruise load. According to our calculated production rates, SOA from airport emissions (idling
328 jet engines) exceeds POA by a factor of 10 already after 3 hours of atmospheric aging and therefore considerably
329 impacts areas downwind of airport emissions. Compared to idling aircraft emissions, aging of vehicle exhaust

emissions results in much lower enhancements, ranging between factors of 5-10 and 1.5-3, for gasoline and diesel vehicles, respectively (Gordon et al., 2014a; 2014b). The NMOG emission factors and SOA potential can be used in conjunction with emission inventories and fuel use data to assess the impact of aircraft emissions on air quality in comparison with other mobile sources. Here, we have considered the Zurich international airport as an example (Switzerland, 23 million passengers in 2010). We note that the influence of the engine type and age on the total NMOG emission rates is minor compared to other parameters (e.g. thrust level). In addition, the engine type tested here is the most frequently used/sold model for commercial aviation. Thus, we believe that the emission rates used here are generally representative of idling aircraft emissions. Combining the recorded aircraft fuel use with the standard LTO cycle and the NMOG EIs measured, we estimate aircraft NMOG emissions in Zurich for 2010 to be in the range of 90–190 tons/year (Kilic et al., 2017). Based on the average SOA bulk yields (SOA/total NMOG) obtained herein (~5-8%), we estimate a total SOA production potential from airport emissions for the area of Zurich to range from 5.4 to 13.2 tons/year. These SOA production potential values can be directly compared to emissions from on-road vehicles derived from the EDGARv4.2 emission inventory, which provides worldwide temporally and spatially resolved NMOG emissions from road vehicles with a grid size of ~200 km². For the grid cell containing Zurich (47.25° North, 8.75° East) the NMOG emissions from on-road vehicles is estimated to be 631 tons/year. While SOA yields from diesel vehicle emissions are expected to be more elevated than those from gasoline car emissions, due to the presence of intermediate volatility species, recent reports suggest these yields to be comparably high, ~15% (Gentner et al., 2017). Using this yield value for emissions from both types of vehicles (Platt et al., 2017), we estimate the total SOA production potential from on road vehicles for the area of Zurich to be ~94 tons/year, 10 fold higher than SOA from aircraft emissions. However, the airport is a point source within this region and thus the relative contribution of the airport emissions to a specific location downwind of this source is significantly higher than implied by this calculation. Although this estimate applies to a specific airport, it does indicate that aircraft NMOG emissions may constitute significant SOA precursors downwind of airports, while other fossil fuel combustion sources dominate urban areas in general.

355 **Acknowledgements**

356 Funding was provided by the Swiss Federal Office of Civil Aviation (FOCA). This project would not have been
357 possible without the support of Rene Richter (PSI) and SR Technics personnel. Many individuals from SR
358 Technics contributed to the project but we owe special thanks to those from the Maintenance and Test Cell Group.
359 JGS acknowledges support from the Swiss National Science Foundation starting grant BSSG10_155846.

361 **References**

- 362 (Alvarez et al., 2009) Alvarez, E. G., Borrás, E., Viidanoja, J., & Hjorth, J. (2009). Unsaturated dicarbonyl
363 products from the OH-initiated photo-oxidation of furan, 2-methylfuran and 3-methylfuran. *Atmos. Environ.*,
364 43(9), 1603–1612.
- 365 (Anderson et al., 2006) Anderson, B. E., Chen, G., & Blake, D. R. (2006). Hydrocarbon emissions from a
366 modern commercial airliner. *Atmos. Environ.*, 40(19), 3601–3612.
- 367 (ASTM, 1996) ASTM, D. (1996). 5291 (1996) standard test methods for instrumental determination
368 of carbon, hydrogen, and nitrogen in petroleum products and lubricants. *ASTM, West Conshohocken*.
- 369 (Barnet et al., 2012) Barnet, P., Dommen, J., DeCarlo, P., Tritscher, T., Praplan, A., Platt, S., Prévôt, A.,
370 Donahue, N., & Baltensperger, U. (2012). OH clock determination by proton transfer reaction mass spectrometry
371 at an environmental chamber. *Atmos. Meas. Tech.*, 5(3), 647–656.
- 372 (Brem et al., 2015) Brem, B. T., Durdina, L., Siegerist, F., Beyerle, P., Bruderer, K., Rindlisbacher, T.,
373 Rocci-Denis, S., Andac, M. G., Zelina, J., Penanhoat, O., & Wang, J. (2015). Effects of fuel aromatic content on
374 nonvolatile particulate emissions of an in-production aircraft gas turbine. *Environ. Sci. Technol.*, 49(22), 13149–
375 13157.
- 376 (Brown et al., 2010) Brown, P., Watts, P., Märk, T., & Mayhew, C. (2010). Proton transfer reaction mass
377 spectrometry investigations on the effects of reduced electric field and reagent ion internal energy on product ion
378 branching ratios for a series of saturated alcohols. *Int. J. Mass Spectrom.*, 294(2), 103–111.
- 379 (Bruns et al., 2015) Bruns, E., El Haddad, I., Keller, A., Klein, F., Kumar, N., Pieber, S., Corbin, J., Slowik,
380 J., Brune, W., Baltensperger, U. & Prévôt, A. S. H. (2015). Inter-comparison of laboratory smog chamber and
381 flow reactor systems on organic aerosol yield and composition. *Atmos. Meas. Tech.*, 8(6), 2315–2332.

382 (Bruns et al., 2016) Bruns, E. A., El Haddad, I., Slowik, J. G., Kilic, D., Klein, F., Baltensperger, U., &
383 Prévôt, A. S. H. (2016). Identification of significant precursor gases of secondary organic aerosols from residential
384 wood combustion. *Sci. Rep.*, 6, 27881, doi:10.1038/srep27881.

385 (Buhr et al., 2002) Buhr, K., van Ruth, S., & Delahunty, C. (2002). Analysis of volatile flavour compounds
386 by proton transfer reaction-mass spectrometry: fragmentation patterns and discrimination between isobaric and
387 isomeric compounds. *Int. J. Mass Spectrom.*, 221(1), 1–7.

388 (Chan et al., 2010) Chan, A., Chan, M., Surratt, J. D., Chhabra, P., Loza, C., Crouse, J., Yee, L., Flagan,
389 R., Wennberg, P., & Seinfeld, J. (2010). Role of aldehyde chemistry and NO_x concentrations in secondary organic
390 aerosol formation. *Atmos. Chem. Phys.*, 10(15), 7169–7188.

391 (Chan et al., 2009) Chan, A. W. H., Kautzman, K. E., Chhabra, P. S., Surratt, J. D., Chan, M. N., Crouse,
392 J. D., Kürten, A., Wennberg, P. O., Flagan, R. C., & Seinfeld, J. H. (2009). Secondary organic aerosol formation
393 from photooxidation of naphthalene and alkylnaphthalenes: implications for oxidation of intermediate volatility
394 organic compounds (IVOCs). *Atmos. Chem. Phys.*, 9(9), 3049–3060.

395 (Chhabra et al., 2011) Chhabra, P., Ng, N., Canagaratna, M., Corrigan, A., Russell, L., Worsnop, D., Flagan,
396 R., & Seinfeld, J. (2011). Elemental composition and oxidation of chamber organic aerosol. *Atmos. Chem. Phys.*,
397 11(17), 8827–8845.

398 (de Gouw & Warneke, 2007) de Gouw, J. & Warneke, C. (2007). Measurements of volatile organic
399 compounds in the Earth's atmosphere using proton-transfer-reaction mass spectrometry. *Mass Spectrom. Rev.*,
400 26(2), 223–257.

401 (Drinovec et al., 2015) Drinovec, L., Mocnik G., Zotter P., Prevot A. S. H., Ruckstuhl C., Coz E., Rupakheti
402 M., Sciare J., Muller T., Wiedensohler A., and Hansen A. D. A. (2015) The "dual-spot" Aethalometer: an
403 improved measurement of aerosol black carbon with real-time loading compensation, *Atmos. Meas. Tech.*, 8(5),
404 1965-1979.

405 (Gentner et al., 2017) Gentner D. R., Shantanu H. Jathar H. S., Gordon D. T., Bahreini R., Day D. A., Imad
406 El Haddad, Hayes P. L., Pieber S. M., Platt S. M., de Gouw J., Goldstein H. A., Harley R. A., Jimenez L. J., Prévôt
407 A. S. H., and Robinson L. A. (2017). Review of urban secondary organic aerosol formation from gasoline and
408 diesel motor vehicle emissions, *Environ. Sci. Technol.*, 51 (3), 1074–1093. doi: 10.1021/acs.est.6b04509

409 (Gordon et al., 2014a) Gordon, T., Presto, A., Nguyen, N., Robertson, W., Na, K., Sahay, K., Zhang, M.,
410 Maddox, C., Rieger, P., Chattopadhyay, S., Maldonado, H., Maricq, M. M., and Robinson, A. L. (2014a).
411 Secondary organic aerosol production from diesel vehicle exhaust: impact of aftertreatment, fuel chemistry and
412 driving cycle. *Atmos. Chem. Phys.*, 14(9), 4643–4659.

413 (Gordon et al., 2014b) Gordon, T. D., Presto, A. A., May, A. A., Nguyen, N. T., Lipsky, E. M., Donahue,
414 N. M., Gutierrez, A., Zhang, M., Maddox, C., Rieger, P., Chattopadhyay, S., Maldonado, H., Maricq, M. M., &
415 Robinson, A. L. (2014b). Secondary organic aerosol formation exceeds primary particulate matter emissions for
416 light-duty gasoline vehicles. *Atmos. Chem. Phys.*, 14(9), 4661–4678.

417 (Gueneron et al., 2015) Gueneron, M., Erickson, M. H., VanderSchelden, G. S., & Jobson, B. T. (2015). PTR-
418 MS fragmentation patterns of gasoline hydrocarbons. *Int. J. Mass Spectrom.*, 379, 97–109.

419 (Herndon et al., 2006) Herndon, S. C., Rogers, T., Dunlea, E. J., Jayne, J. T., Miake-Lye, R., & Knighton, B.
420 (2006). Hydrocarbon emissions from in-use commercial aircraft during airport operations. *Environ. Sci. Technol.*,
421 40(14), 4406–4413.

422 (Hildebrandt et al., 2009) Hildebrandt, L., Donahue, N. M., & Pandis, S. N. (2009). High formation of secondary
423 organic aerosol from the photo-oxidation of toluene. *Atmos. Chem. Phys.*, 9(9), 2973–2986.

424 (Hudda & Fruin, 2016) Hudda, N. & Fruin, S. (2016). International airport impacts to air quality: Size and
425 related properties of large increases in ultrafine particle number concentrations. *Environ. Sci. Technol.*, 50(7),
426 3362–3370.

427 (Hudda et al., 2014) Hudda, N., Gould, T., Hartin, K., Larson, T. V., & Fruin, S. A. (2014). Emissions from
428 an international airport increase particle number concentrations 4-fold at 10 km downwind. *Environ. Sci. Technol.*,
429 48(12), 6628–6635.

430 (Hudda et al., 2016) Hudda, N., Simon, M., Zamore, W., Brugge, D., & Durant, J. (2016). Aviation
431 emissions impact ambient ultrafine particle concentrations in the Greater Boston area. *Environ. Sci. Technol.*,
432 2016, 50 (16), 8514–8521.

433 (Jordan et al., 2009) Jordan, A., Haidacher, S., Hanel, G., Hartungen, E., Märk, L., Seehauser, H.,
434 Schottkowsky, R., Sulzer, P., & Märk, T. (2009). A high resolution and high sensitivity proton-transfer-reaction
435 time-of-flight mass spectrometer (PTR-ToF-MS). *Int. J. Mass Spectrom.*, 286(2), 122–128.

436 (Kang et al., 2007) Kang, E., Root, M., Toohey, D., & Brune, W. (2007). Introducing the concept of
437 potential aerosol mass (PAM). *Atmos. Chem. Phys.*, 7(22), 5727–5744.

438 (Kilic et al., 2017) Kilic, D., Brem, B. T., Klein, F., El-Haddad, I., Durdina, L., Rindlisbacher, T., Setyan,
439 A., Huang, R., Wang, J., Slowik, J. G., Baltensperger, U., & Prevot, A. S. H. (2017). Characterization of gas-
440 phase organics using proton transfer reaction time-of-flight mass spectrometry: Aircraft turbine engines. *Environ.*
441 *Sci. Technol.*, 2017, 51 (7), 3621–3629. doi: 10.1021/acs.est.6b04077

442 (Kim, 2009) Kim, B. Y. (2009). Guidebook on Preparing Airport Greenhouse Gas Emissions
443 Inventories, volume 11. *Transportation Research Board*.

444 (Kinsey et al., 2010) Kinsey, J. S., Dong, Y., Williams, D. C., & Logan, R. (2010). Physical characterization
445 of the fine particle emissions from commercial aircraft engines during the aircraft particle emissions experiment
446 (APEX) 1–3. *Atmos. Environ.*, 44(17), 2147–2156.

447 (Kuenen et al., 2014) Kuenen, J. J. P., Visschedijk, A. J. H., Jozwicka, M., & Denier van der Gon, H. A. C.
448 (2014). TNO-MACC_II emission inventory; a multi-year (2003–2009) consistent high-resolution European
449 emission inventory for air quality modelling. *Atmos. Chem. Phys.*, 14(20), 10963–10976.

450 (Lambe et al., 2015) Lambe, A., Chhabra, P., Onasch, T., Brune, W., Hunter, J., Kroll, J., Cummings, M.,
451 Brogan, J., Parmar, Y., Worsnop, D., et al. (2015). Effect of oxidant concentration, exposure time, and seed
452 particles on secondary organic aerosol chemical composition and yield. *Atmos. Chem. Phys.*, 15(6), 3063–3075.

453 (Liati et al., 2014) Liati, A., Brem, B. T., Durdina, L., Vöggtli, M., Dasilva, Y. A. R., Eggenchwiler, P. D.,
454 & Wang, J. (2014). Electron microscopic study of soot particulate matter emissions from aircraft turbine engines.
455 *Environ. Sci. Technol.*, 48(18), 10975–10983.

456 (Lin et al., 2008) Lin, S., Munsie, J., Herdt-Losavio, M., Hwang, S., Civerolo, K., McGarry, K., &
457 Gentile, T. (2008). Residential proximity to large airports and potential health impacts in New York State. *Int.*
458 *Arch. Occup. Environ. Health.*, 81(7), 797–804.

459 (Mao et al., 2009) Mao, J., Ren, X., Brune, W., Olson, J., Crawford, J., Fried, A., Huey, L., Cohen, R.,
460 Heikes, B., Singh, H., et al. (2009). Airborne measurement of OH reactivity during INTEX-B. *Atmos. Chem.*
461 *Phys.*, 9(1), 163–173.

462 (Miracolo et al., 2011) Miracolo, M., Hennigan, C., Ranjan, M., Nguyen, N., Gordon, T., Lipsky, E., Presto,
463 A., Donahue, N., & Robinson, A. (2011). Secondary aerosol formation from photochemical aging of aircraft
464 exhaust in a smog chamber. *Atmos. Chem. Phys.*, 11(9), 4135–4147.

465 (Miracolo et al., 2012) Miracolo, M. A., Drozd, G. T., Jathar, S. H., Presto, A. A., Lipsky, E. M., Corporan,
466 E., & Robinson, A. L. (2012). Fuel composition and secondary organic aerosol formation: Gas-turbine exhaust
467 and alternative aviation fuels. *Environ. Sci. Technol.*, 46(15), 8493–8501.

468 (Nakao et al., 2011) Nakao, S., Clark, C., Tang, P., Sato, K., & Cocker III, D. (2011). Secondary organic
469 aerosol formation from phenolic compounds in the absence of NO_x. *Atmos. Chem. Phys.*, 11(20), 10649–10660.

470 (Ng et al., 2007) Ng, N., Kroll, J., Chan, A., Chhabra, P., Flagan, R., & Seinfeld, J. (2007). Secondary
471 organic aerosol formation from m-xylene, toluene, and benzene. *Atmos. Chem. Phys.*, 7(14), 3909–3922.

472 (Odum et al., 1997) Odum, J. R., Jungkamp, T. P. W., Griffin, R. J., Forstner, H. J. L., Flagan, R. C., &
473 Seinfeld, J. H. (1997). Aromatics, reformulated gasoline, and atmospheric organic aerosol formation. *Environ.*
474 *Sci. Technol.*, 31(7), 1890–1897.

475 Palm, B. B., Campuzano-Jost, P., Ortega, A. M., Day, D. A., Kaser, L., Jud, W., Karl, T., Hansel, A., Hunter, J.
476 F., Cross, E. S., Kroll, J. H., Peng, Z., Brune, W. H., and Jimenez, J. L.: In situ secondary organic aerosol formation
477 from ambient pine forest air using an oxidation flow reactor, *Atmos. Chem. Phys.*, 16, 2943–2970,
478 <https://doi.org/10.5194/acp-16-2943-2016>, 2016.

479 (Peng et al., 2016) Peng, Z., Day, D. A., Ortega, A. M., Palm, B. B., Hu, W., Stark, H., Li, R., Tsigaridis,
480 K., Brune, W. H., & Jimenez, J. L. (2016). Non-OH chemistry in oxidation flow reactors for the study of
481 atmospheric chemistry systematically examined by modeling. *Atmos. Chem. Phys.*, 16(7), 4283–4305.

482 (Peng et al., 2015) Peng, Z., Day, D. A., Stark, H., Li, R., Lee-Taylor, J., Palm, B. B., Brune, W. H., &
483 Jimenez, J. L. (2015). HO_x radical chemistry in oxidation flow reactors with low-pressure mercury lamps
484 systematically examined by modeling. *Atmos. Meas. Tech.*, 8(11), 4863–4890.

485 (Pieber et al., 2017) Simone M. Pieber, Nivedita K. Kumar, Felix Klein, Pierre Comte, Deepika Bhattu,
486 Josef Dommen, Emily A. Bruns, Dogushan Kilic, Alejandro Keller, Urs Baltensperger, Jan Czerwinski, Norbert
487 Heeb, Jay G. Slowik and André S. H. Prévôt. Gas phase composition and secondary organic aerosol formation
488 from gasoline direct injection vehicles investigated in a batch and flow reactor: effects of prototype gasoline
489 particle filters. *Atmos. Chem. Phys. Discuss.*, in review, 2017.

490 (Platt et al., 2013) Platt, S. M., El Haddad, I., Zardini, A. A., Clairotte, M., Astorga, C., Wolf, R., Slowik,
491 J. G., Temime-Roussel, B., Marchand, N., Ježek, I., Drinovec, L., Močnik, G., Möhler, O., Richter, R., Barmet,
492 P., Bianchi, F., Baltensperger, U., & Prévôt, A. S. H. (2013). Secondary organic aerosol formation from gasoline
493 vehicle emissions in a new mobile environmental reaction chamber. *Atmos. Chem. Phys.*, 13(18), 9141–9158.

494 (Platt et al., 2014) Platt, S. M., El Haddad, I., Pieber, S. M., Huang, R.-J., Zardini, A., Clairotte, M.,
495 Suarez-Bertoa, R., Barmet, P., Pfaffenberger, L., Wolf, R., Slowik, J. G., Fuller, S. J., Kalberer, M., Chirico, R.,
496 Dommen, J., Astorga, C., Zimmermann, N., Marchand, N., Hellebust, S., Temime-Roussel, B., Baltensperger, U.
497 & Prévôt, A. S. H. (2014). Two-stroke scooters are a dominant source of air pollution in many cities, *Nat.*
498 *Commun.*, 5, 3749.

499 (Platt et al., 2017) Platt, S. M., El Haddad, I., Pieber, S. M., Zardini, A., Clairotte, M., Suarez-Bertoa R.,
500 Daellenbach, K.R., Huang, R.-J., Slowik, J. G., Hellebust S., Temime-Roussel B., Marchand N., de Gouw J.,
501 Jimenez J.L., Hayes P. L., Robinson A. L., Baltensperger U., Astorga C. Prévôt, A. S. H. (2017). Gasoline cars
502 produce more carbonaceous particulate matter than modern filter-equipped diesel cars, *Sci. Rep.*, 7, 4926.

503 (Presto et al., 2010) Presto, A. A., Miracolo, M. A., Donahue, N. M., & Robinson, A. L. (2010). Secondary
504 organic aerosol formation from high-NO_x photo-oxidation of low volatility precursors: n-alkanes. *Environ. Sci.*
505 *Technol.*, 44(6), 2029–2034.

506 (Robinson et al., 2007) Robinson, A. L., Donahue, N. M., Shrivastava, M. K., Weitkamp, E. A., Sage, A. M.,
507 Grieshop, A. P., Lane, T. E., Pierce, J. R., & Pandis, S. N. (2007). Rethinking organic aerosols: Semivolatile
508 emissions and photochemical aging. *Science*, 315(5816), 1259–1262.

509 (Shakya & Griffin, 2010) Shakya, K. M. & Griffin, R. J. (2010). Secondary organic aerosol from photooxidation
510 of polycyclic aromatic hydrocarbons. *Environ. Sci. Technol.*, 44(21), 8134–8139.

511 (Slemr et al., 2001) Slemr, F., Giehl, H., Habram, M., Slemr, J., Schlager, H., Schulte, P., Haschberger, P.,
512 Lindermeir, E., Döpelheuer, A., & Plohr, M. (2001). In-flight measurement of aircraft CO and nonmethane
513 hydrocarbon emission indices. *J. Geophys. Res.: Atmos.*, 106(D7), 7485–7494.

514 (Spicer et al., 1994) Spicer, C., Holdren, M., Riggin, R., & Lyon, T. (1994). Chemical composition and
515 photochemical reactivity of exhaust from aircraft turbine engines. In *Ann. Geophys.*, 12, 944–955.

516 (Stirnweis et al., 2017) Stirnweis, L., Marcolli, C., Dommen, J., Barmet, P., Frege, C., Platt, S. M., Bruns, E.
517 A., Krapf, M., Slowik, J. G., Wolf, R., Prévôt, A. S. H., Baltensperger, U., and El-Haddad, I.: Assessing the
518 influence of NO_x concentrations and relative humidity on secondary organic aerosol yields from α-pinene photo-
519 oxidation through smog chamber experiments and modelling calculations, *Atmos. Chem. Phys.*, 17, 5035-5061,
520 <https://doi.org/10.5194/acp-17-5035-2017>, 2017.

521 (Tkacik et al., 2012) Tkacik, D. S., Presto, A. A., Donahue, N. M., & Robinson, A. L. (2012). Secondary
522 organic aerosol formation from intermediate-volatility organic compounds: cyclic, linear, and branched alkanes.
523 *Environ. Sci. Technol.*, 46(16), 8773–8781.

524 (Unal et al., 2005) Unal, A., Hu, Y., Chang, M. E., Odman, M. T., & Russell, A. G. (2005). Airport related
525 emissions and impacts on air quality: Application to the Atlanta International Airport. *Atmos. Environ.*, 39(32),
526 5787 – 5798.

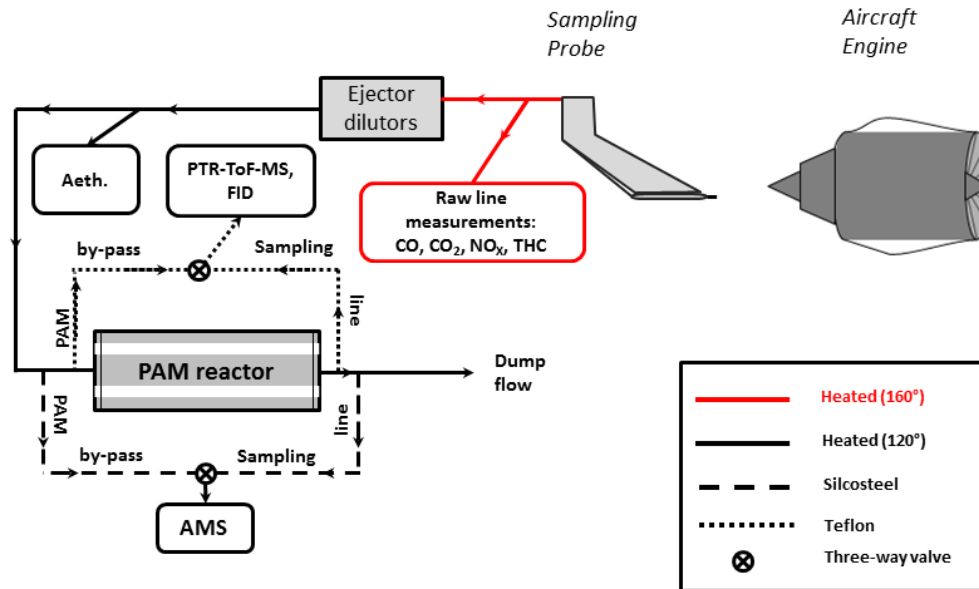
527 (Westerdahl et al., 2008) Westerdahl, D., Fruin, S. A., Fine, P. L., & Sioutas, C. (2008). The Los Angeles
528 International Airport as a source of ultrafine particles and other pollutants to nearby communities. *Atmos.*
529 *Environ.*, 42(13), 3143–3155.

530 (Yee et al., 2013) Yee, L., Kautzman, K., Loza, C., Schilling, K., Coggon, M., Chhabra, P., Chan, M.,
531 Chan, A., Hersey, S., Crouse, J., et al. (2013). Secondary organic aerosol formation from biomass burning
532 intermediates: phenol and methoxyphenols. *Atmos. Chem. Phys.*, 13(16), 8019–8043.

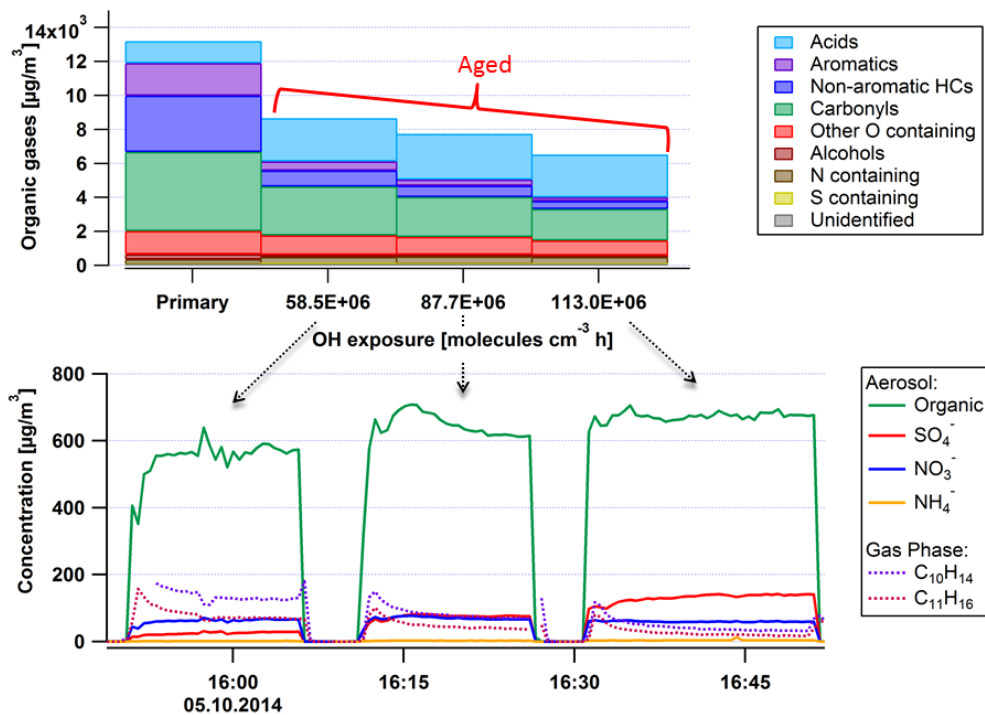
533 (Yu et al., 2010) Yu, Z., Liscinsky, D.S., Winstead, E.L., True, B.S., Timko, M.T., Bhargava, A.,
 534 Herndon, S.C., Miake-Lye, R.C. and Anderson, B.E., 2010. Characterization of lubrication oil emissions from
 535 aircraft engines. *Environ. Sci. Technol.*, 44(24), 9530-9534.

536 (Yu et al., 2012) Yu, Z., Herndon, S.C., Ziemba, L.D., Timko, M.T., Liscinsky, D.S., Anderson, B.E.
 537 and Miake-Lye, R.C., 2012. Identification of lubrication oil in the particulate matter emissions from engine
 538 exhaust of in-service commercial aircraft. *Environ. Sci. Technol.*, 46(17), 9630-9637.

539
 540

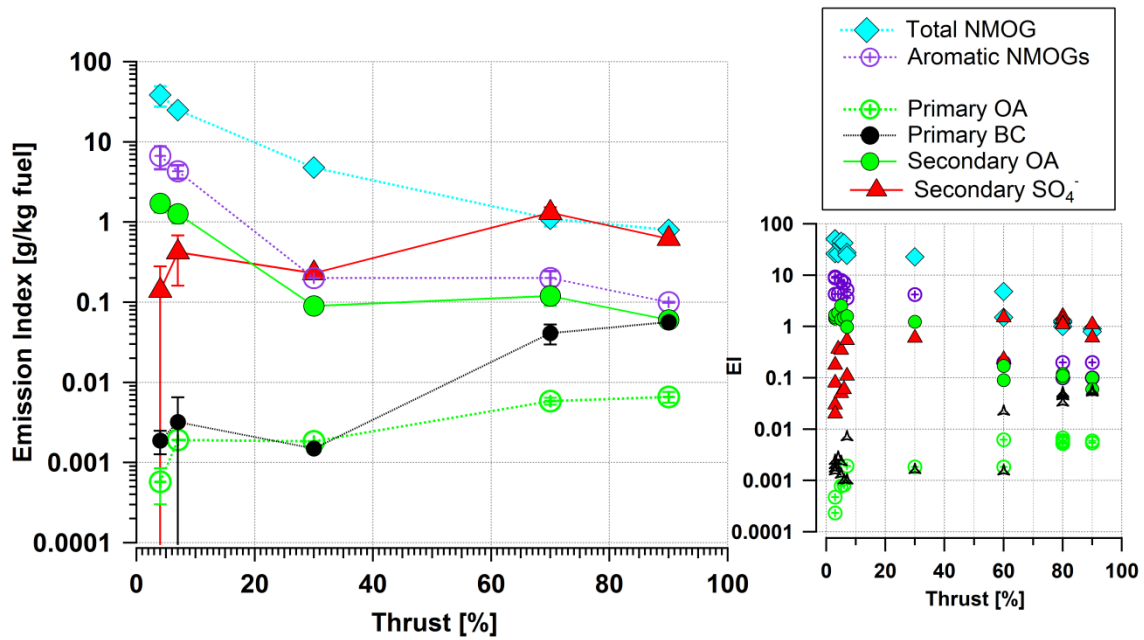


541
 542 **Figure 1: Simplified scheme of the experimental setup.**



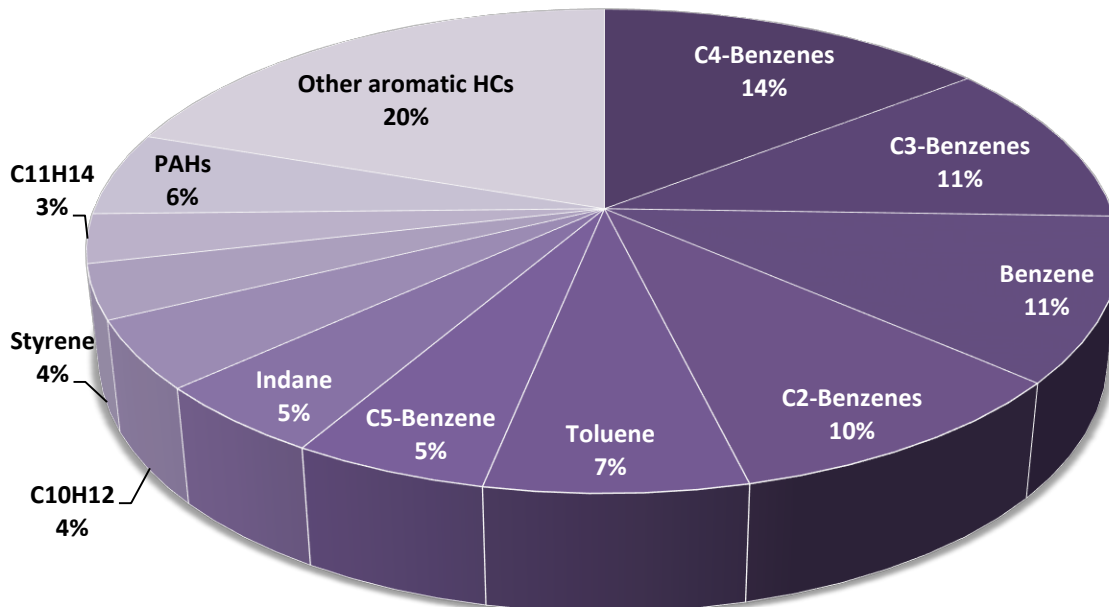
543
 544 **Figure 2: Sample experiment showing mean NMOG emissions (top) and representative time series**
 545 **for particle and NMOG components (bottom) for varying OH exposures.** Hydrocarbon concentrations
 546 (non-aromatic HCs (dark blue), aromatic HCs (purple) and carbonyls (green) decrease in the PAM while
 547 the concentrations of acids (mostly formic and acetic ~90% of the total acids) increase. The bottom panel

548 shows the aerosol (Organic, SO₄, NO₃, NH₄) formed and gaseous aromatics (C₁₀H₁₄, C₁₁H₁₆) for the
 549 different OH exposures in the PAM given in the top panel.



550
 551 **Figure 3: Average emission indices (left) and EIs from individual test points (right) for primary non-**
 552 **methane organic gases (NMOGs), aromatic gases, primary organic aerosol (POA), equivalent black**
 553 **carbon (BC), secondary organic aerosol (SOA), nitrate (NO₃) and sulfate (SO₄).** Error bars (+/-) are the
 554 standard deviations of the means with a confidence interval of 95%. The OH exposure was in the range
 555 of 91-113 x 10⁶ molecule cm⁻¹ h for the secondary aerosol cases.

556
 557



558
 559 **Figure 4: Mass fractions of aromatic compounds for primary emissions (directly emitted) at idle**
 560 **(thrust 3-7%). Benzene derivatives, xylenes, tri-, tetra-, pentamethylbenzene, benzene and toluene**
 561 **account for ~60% of all aromatics.**

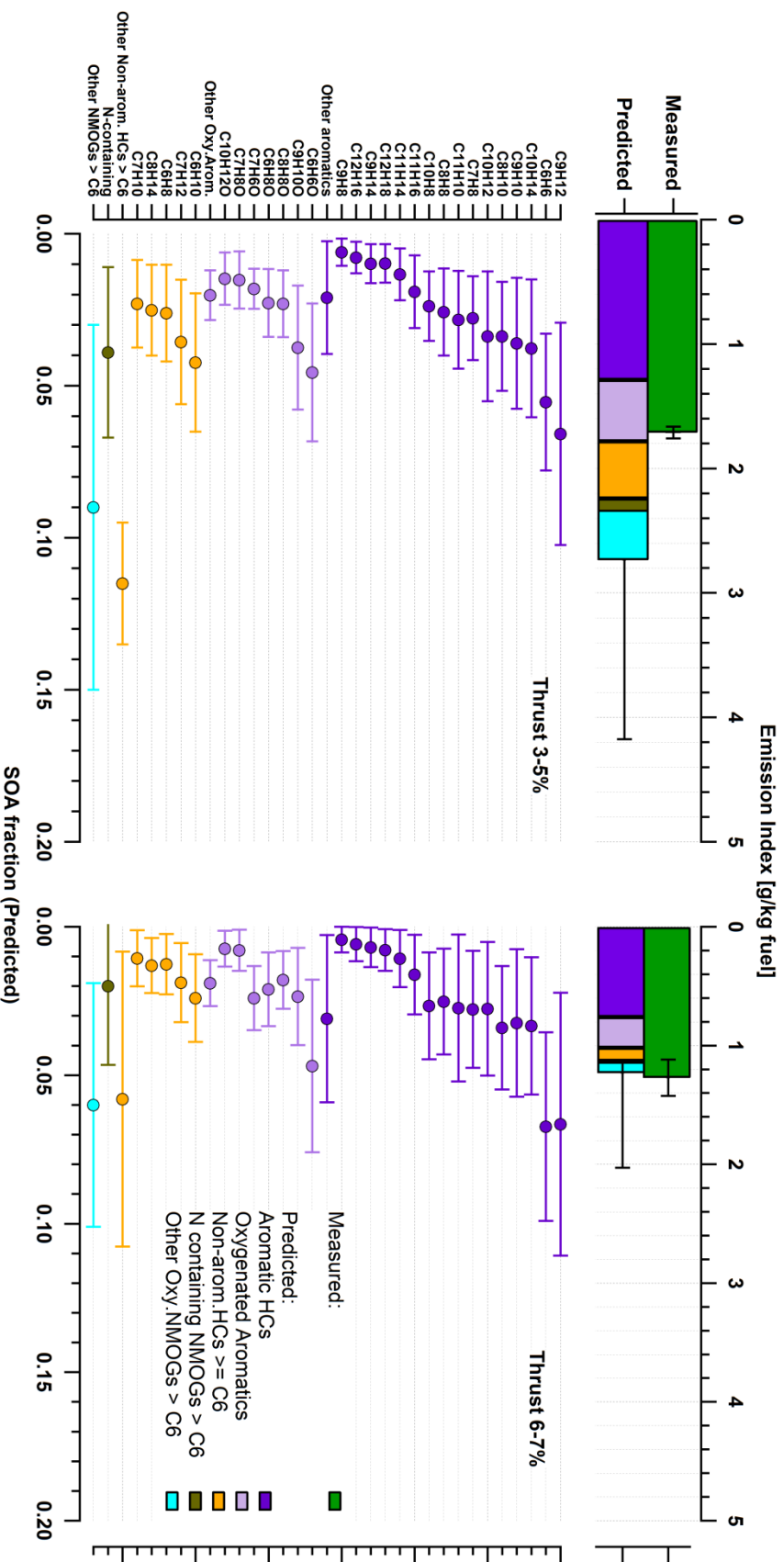


Figure 5: Comparison of the SOA measured by the AMS and the SOA predicted by the oxidation of NMOGs (top panel). The statistics are presented for low load idling (thrust 3-5%) on the left half and for idling 6-7% on the right. Aromatic hydrocarbons (purple) were the most abundant precursors of SOA at idle (thrust 3-7%) explaining all SOA formed (green, top panel) at thrust 3-5% and most (~90%) at thrust 6-7%. Aromatic SOA comprised the largest fraction followed by oxygenated aromatics (light purple - e.g. phenol, benzaldehydes), non-aromatic hydrocarbons (orange) with more than 6 carbon atoms in their molecular structure (non-arom. HCS \geq C6), nitrogen containing compounds (brown), other oxygenated-NMOGs $>$ C6 (cyan). Average fractions of individual NMOGs (bottom panel) were calculated by using SOA yields from literature (see *Table 2*) and the amount of NMOG reacted. Error bars show standard deviations of the means (CI: 95%).

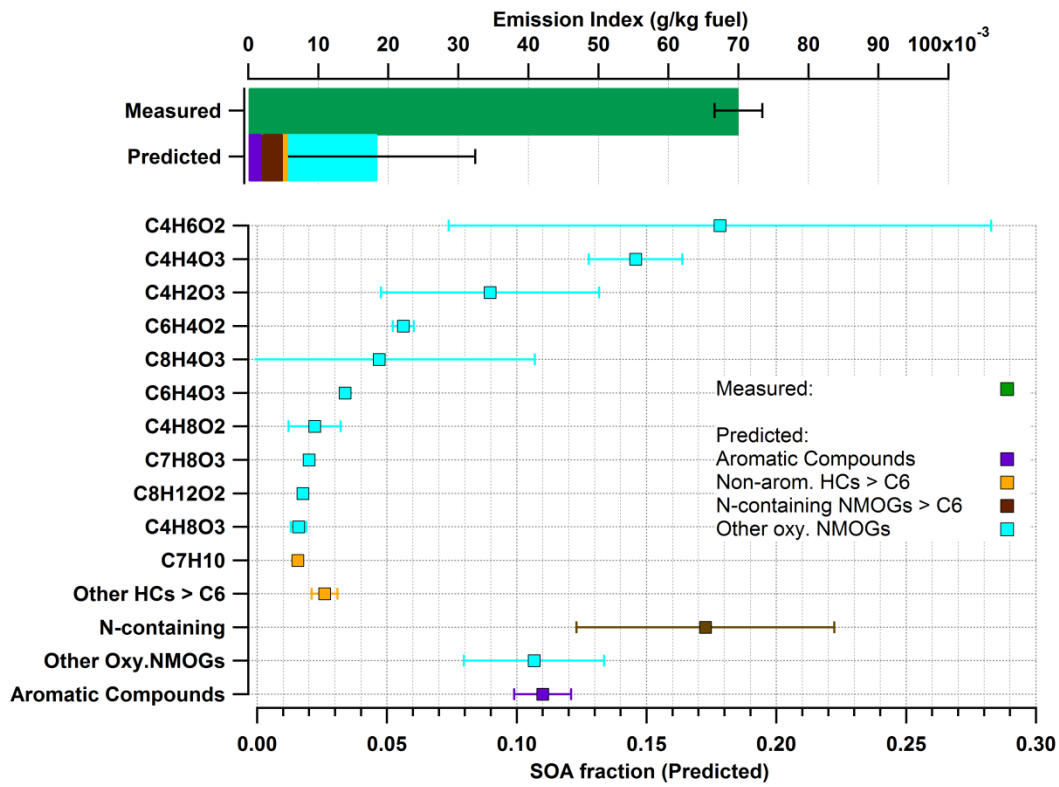


Figure 6: Measured and predicted SOA comparison at an approximated cruise load, using the same approach as in Fig. 5. In contrast to idle conditions, total NMOGs detected do not explain SOA formed.

Table 1: Volume mixing ratios of gaseous emissions, engine parameters and emission indices (EIs) for primary (directly emitted) and secondary (after aging) for all experiments.

Thrust (%)	Fuel Consumption (kg/sec)	Primary								Aged		
		CO ₂ (ppmv)	CO (ppmv)	THC (ppmvC)	NO _x (ppmv)	NMOG (g/kg fuel)	Aromatic Gases (g/kg fuel)	BC (g/kg fuel)	POA (g/kg fuel)	SO ₄ (g/kg fuel)	OH exposure (molec. cm ⁻³ h)	SOA (g/kg fuel)
3	0.09	1863	764	239	14	51	9.4	1.70E-03	2.34E-04	0.03	8.80E+07	1.4
3	0.09	1831	766	244	14	51	8.8	2.00E-03	4.74E-04	0.02	8.80E+07	n/a
3	0.09	1560	709	222	14	26	4.3	1.50E-03	<2.0E-03	0.08	6.00E+07	1.5
3	0.09	1560	709	222	14	26	4.3	2.40E-03	<2.0E-03	0.18	9.00E+07	1.7
3	0.09	1560	709	222	14	26	4.3	2.80E-03	<2.0E-03	0.37	1.13E+08	1.9
4	n/a	1884	543	173	n/a	39	7.7	2.30E-03	<2.0E-03	0.35	1.00E+08	2.6
5	0.11	1829	442	114	17	46	7.9	1.30E-03	7.81E-04	0.05	8.80E+07	1.4
5	0.11	1758	422	98	17	42	7.1	1.00E-03	8.13E-04	0.06	8.80E+07	1.5
6	0.12	1934	410	113	21	28	5.2	1.00E-03	<2.0E-03	0.54	1.00E+08	1.6
7	0.14	1909	168	45	23	25	3.6	7.00E-03	1.91E-03	0.11	8.80E+07	1.0
7	0.14	1978	385	94	23	23	4.2	1.60E-03	<2.0E-03	0.6	1.00E+08	1.2
30	0.31	2953	40	8	62	5	0.2	1.50E-03	1.84E-03	0.23	8.80E+07	0.1
60	0.65	3709	12	7	131	2	0.2	2.20E-02	6.21E-03	1.51	8.50E+07	0.2
60	0.65	3709	12	7	131	1	0.2	3.30E-02	6.80E-03	1.61	8.50E+07	0.1
80	0.9	4344	16	6	195	1	0.1	4.60E-02	5.55E-03	1.39	1.00E+08	0.1
80	0.9	4291	14	7	195	1	0.2	4.40E-02	6.01E-03	1.16	8.50E+07	0.1
80	0.9	4291	14	7	195	1	0.2	5.00E-02	5.24E-03	1.1	8.50E+07	0.1
80	0.9	4291	14	7	195	1	0.2	5.20E-02	5.37E-03	1.1	8.50E+07	0.1
90	1.1	4657	16	6	202	1	0.1	5.50E-02	5.89E-03	0.61	8.50E+07	0.1
90	1.1	4657	16	6	202	1	0.1	5.80E-02	7.30E-03	0.63	8.50E+07	0.1

Table 2. Precursor OGs, their corresponding functional group and protonated m/z, SOA yield coefficients* from literature, and average SOA EI estimated for different thrusts.

VOC formula	m/z	Group	SOA yield*	SOA Emission Index (g/kg fuel)			
				Thrust 3-5%		Thrust 6-7%	
				Average	±	Average	±
(C ₉ H ₁₂)H ⁺	121.101	Aromatic	0.32	0.19	0.11	0.07	0.04
(C ₆ H ₆)H ⁺	79.054	Aromatic	0.33	0.16	0.06	0.07	0.03
(C ₁₀ H ₁₄)H ⁺	135.117	Aromatic	0.2	0.11	0.07	0.03	0.02
(C ₉ H ₁₀)H ⁺	119.086	Aromatic	0.32	0.10	0.06	0.03	0.02
(C ₈ H ₁₀)H ⁺	107.086	Aromatic	0.2	0.10	0.05	0.04	0.02
(C ₁₀ H ₁₂)H ⁺	133.101	Aromatic	0.32	0.10	0.06	0.03	0.02
(C ₇ H ₈)H ⁺	93.070	Aromatic	0.24	0.08	0.04	0.03	0.02
(C ₁₁ H ₁₀)H ⁺	143.086	Aromatic	0.52	0.08	0.05	0.03	0.02
(C ₈ H ₈)H ⁺	105.070	Aromatic	0.32	0.07	0.04	0.03	0.02
(C ₁₀ H ₈)H ⁺	129.070	Aromatic	0.52	0.07	0.03	0.03	0.02
(C ₁₁ H ₁₆)H ⁺	149.132	Aromatic	0.2	0.05	0.03	0.02	0.01
(C ₁₁ H ₁₄)H ⁺	147.117	Aromatic	0.2	0.04	0.02	0.01	0.01
(C ₁₂ H ₁₈)H ⁺	163.148	Aromatic	0.2	0.03	0.02	0.01	0.01
(C ₉ H ₁₄)H ⁺	123.117	Aromatic	0.2	0.03	0.02	0.01	0.01
(C ₁₂ H ₁₆)H ⁺	161.132	Aromatic	0.2	0.02	0.01	0.01	0.01
(C ₉ H ₈)H ⁺	117.070	Aromatic	0.2	0.02	0.01	0.00	0.00
Other	-	Aromatic	0.2	0.06	0.05	0.00	0.00
(C ₆ H ₆ O)H ⁺	95.049	Oxy-arom	0.44	0.13	0.07	0.05	0.03
(C ₆ H ₈ O)H ⁺	97.065	Oxy-arom	0.32	0.07	0.03	0.02	0.01
(C ₇ H ₆ O)H ⁺	107.049	Oxy-arom	0.32	0.05	0.02	0.02	0.01
(C ₆ H ₆ O ₂)H ⁺	111.044	Oxy-arom	0.39	0.03	0.01	0.01	0.00
(C ₁₀ H ₁₂ O ₂)H ⁺	165.091	Oxy-arom	0.2	0.00	0.00	0.00	0.00
(C ₁₀ H ₁₄ O ₂)H ⁺	167.107	Oxy-arom	0.2	0.00	0.00	0.00	0.00
Other NMOGs	> 79.054	Other NMOG	0.15	1.15	0.74	0.20	0.02

*SOA yields from (Ng et al., 2007; Alvarez et al., 2009; Chan et al., 2009 ; 2010; Hildebrandt et al., 2009; Shakya and Griffin, 2010; Chhabra et al., 2011; Nakao et al., 2011; Yee et al., 2013)